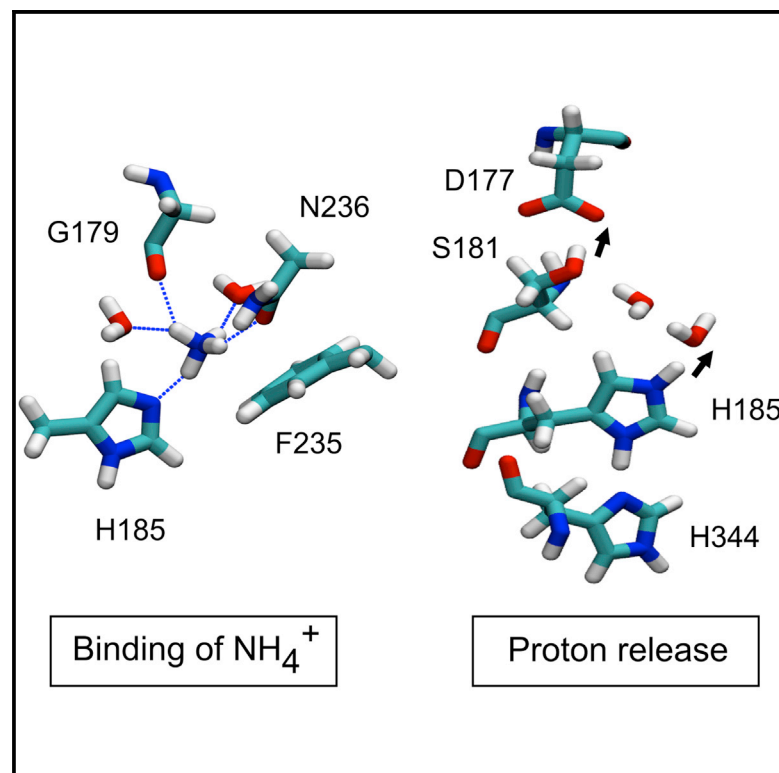# Structure

Mechanism of NH$_4^+$ Recruitment and NH$_3$ Transport in Rh Proteins

Graphical Abstract

Authors

Sefer Baday, Esam A. Orabi, Shihao Wang, Guillaume Lamoureux, Simon Bernèche

Correspondence

simon.berneche@isb-sib.ch (S.B.), guillaume.lamoureux@concordia.ca (G.L.)

In Brief

Using molecular and quantum mechanic simulations, Baday et al show that the RhCG protein transports NH$_3$ but actually recruits NH$_4^+$. The substrate transfers a proton to a signature histidine and diffuses further as NH$_3$. The transferred proton is shuttled back to the extracellular side, resulting in a net electroneutral transport.

Highlights

- Rh proteins transport NH$_3$ but recruit NH$_4^+$

- Signature histidine dyad accepts a proton from NH$_4^+$

- Proton is shuttled back to extracellular space through conserved polar residues

- Proton release from histidine is the rate-limiting step of the transport mechanism

CellPress

Mechanism of NH$_4^+$ Recruitment and NH$_3$ Transport in Rh Proteins

Sefer Baday,[1,2] Esam A. Orabi,[3] Shihao Wang,[3] Guillaume Lamoureux,[3,*] and Simon Bernèche[1,2,*]

[1]SIB Swiss Institute of Bioinformatics, Klingelbergstrasse 50/70, 4056 Basel, Switzerland
[2]Biozentrum, University of Basel, Klingelbergstrasse 50/70, 4056 Basel, Switzerland
[3]Department of Chemistry and Biochemistry, Centre for Research in Molecular Modeling (CERMM), Concordia University, 7141 Sherbrooke Street West, Montréal, QC H4B 1R6, Canada
*Correspondence: simon.berneche@isb-sib.ch (S.B.), guillaume.lamoureux@concordia.ca (G.L.)
http://dx.doi.org/10.1016/j.str.2015.06.010

SUMMARY

In human cells, membrane proteins of the rhesus (Rh) family excrete ammonium and play a role in pH regulation. Based on high-resolution structures, Rh proteins are generally understood to act as NH$_3$ channels. Given that cell membranes are permeable to gases like NH$_3$, the role of such proteins remains a paradox. Using molecular and quantum mechanical calculations, we show that a crystallographically identified site in the RhCG pore actually recruits NH$_4^+$, which is found in higher concentration and binds with higher affinity than NH$_3$, increasing the efficiency of the transport mechanism. A proton is transferred from NH$_4^+$ to a signature histidine (the only moiety thermodynamically likely to accept a proton) followed by the diffusion of NH$_3$ down the pore. The excess proton is circulated back to the extracellular vestibule through a hydrogen bond network, which involves a highly conserved and functionally important aspartic acid, resulting in the net transport of NH$_3$.

INTRODUCTION

Ammonium is a nitrogen source for bacteria, yeast, and plants, which rely on proteins of the Amt/Mep family to uptake ammonium at low extracellular concentrations (Ninnemann et al., 1994; Marini et al., 1997; Ludewig et al., 2002; Siewe et al., 1996). In mammals, erythrocytic RhAG and non-erythrocytic RhBG and RhCG from the rhesus (Rh) family of proteins mediate ammonium transport (Ludewig, 2004; Ripoche et al., 2004; Mouro-Chanteloup et al., 2010) to prevent toxic accumulation of ammonium produced notably by glutamine metabolism.

It remains a matter of debate whether it is the neutral (NH$_3$) or the charged (NH$_4^+$) form of the substrate that is transported by Amt and Rh proteins (Javelle et al., 2007; Weiner and Verlander, 2014). All structures of Amt and Rh proteins elucidated so far reveal a hydrophobic pore that prevents the translocation of charged ammonium (NH$_4^+$), which suggests that both protein families transport neutral ammonia (NH$_3$) (Khademi et al.,

2004; Zheng et al., 2004; Andrade et al., 2005; Lupo et al., 2007; Gruswitz et al., 2010). However, functional studies paint a more complex picture. The measurement of electric current provides strong evidence that Amt proteins transport NH$_4^+$ (Ludewig et al., 2002; Wacker et al., 2014), although the closely related prokaryotic homolog AmtB from *E. coli* was reported to transport NH$_3$ (Khademi et al., 2004; Javelle et al., 2005), a view that was later challenged (Javelle et al., 2007). The debate is more open in the case of Rh proteins, which were reported to transport NH$_3$ (Ludewig, 2004; Ripoche et al., 2004; Mouro-Chanteloup et al., 2010) or NH$_4^+$ (Hemker et al., 2003; Nakhoul et al., 2005, 2010) or both (Bakouh et al., 2004; Benjelloun et al., 2005).

Amt and Rh proteins share many structural features, but important differences between their structures could support functional differences (Zidi-Yahiaoui et al., 2009; Baday et al., 2013). The hydrophobic pore of RhCG (Gruswitz et al., 2010) is lined with two histidines (His185 and His344) and is closed on the extracellular side by two phenylalanine residues (Phe130 and Phe235), as in Amt proteins (Khademi et al., 2004; Andrade et al., 2005). However, the conformation of the phenylalanine side chains is different in the two classes of proteins: in Amts, the two aromatic cycles are predominantly parallel and create a barrier that notably blocks water access to the histidine dyad, while in RhCG they are in a perpendicular conformation and line a hydrophilic pore reaching down to His185 (Figures 1A and 1B) (Baday et al., 2013). In Amts, a tryptophan residue (Trp148 in AmtB) defines an NH$_4^+$ recruitment site above the two phenylalanine residues. In RhCG, this tryptophan is replaced by a leucine (Leu170) the smaller side chain of which, combined with a slightly different orientation of the helices in that region, allows for a wider pore in which water molecules can diffuse and reach the histidine dyad. Moreover, a phenylalanine residue (Phe74) is found at the level of the histidine dyad in RhCG, further differentiating its pore from that of Amt proteins, in which less bulky valine or isoleucine allows for the transient formation of a continuous water chain in the pore. Our recent study suggests that these structural differences lead to different hydration patterns that are likely to be determinant of the transport mechanisms (Baday et al., 2013).

There is a consensus that Amt proteins present a recruitment site with high binding affinity for NH$_4^+$, which needs to deprotonate for permeation to take place (Lin et al., 2006; Luzhkov et al., 2006; Bostick and Brooks, 2007; Nygaard et al., 2006; Wang et al., 2012). There is, however, a debate on the deprotonation
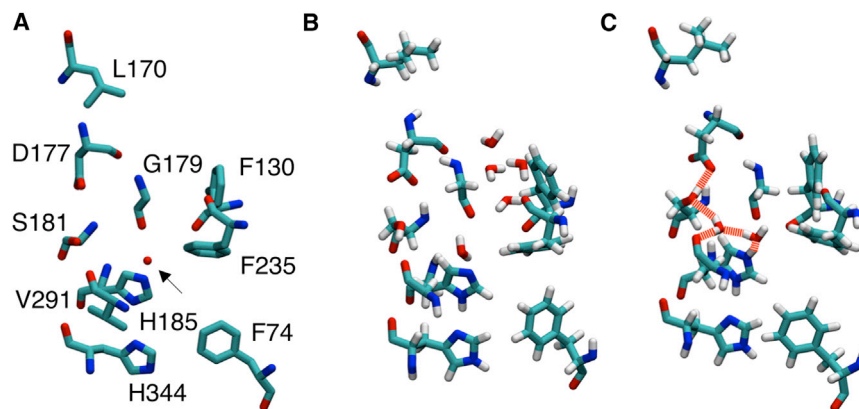
Figure 1. Molecular Representations of the RhCG Pore

(A) The X-ray structure (PDB: 3HD6) is shown with key residues labeled and a crystallographic water indicated by an arrow.

(B) A conformation extracted from an MD simulation shows water of the pore reaching His185.

(C) When His185 is protonated a network of hydrogen bonds forms from His185 Nε atom to Asp177 carboxyl group.

mechanism. It has been proposed that NH_4^+ deprotonates on the extracellular side of the pore, allowing for the net transport of NH_3 (Lin et al., 2006; Luzhkov et al., 2006; Bostick and Brooks, 2007; Nygaard et al., 2006). We have rather proposed that NH_4^+ transfers a proton to the signature histidine dyad, followed by diffusion of NH_3 down the hydrophobic pore, and the transport of the excess proton through a water wire filling this pore (Wang et al., 2012). The overall process results in the net transport of NH_4^+, in agreement with the bulk of functional studies on Amt proteins (Ninnemann et al., 1994; Siewe et al., 1996; Marini et al., 1997; Ludewig et al., 2002; Wacker et al., 2014), and supported by other free energy calculations on Amt-1 (Ullmann et al., 2012).

In the case of Rh proteins, interpretation of the structural data suggests that the transport mechanism simply involves the diffusion of NH_3 down its gradient (Hub et al., 2010). Given that NH_3 can diffuse through membranes, which present a surface area much larger than that of the pore of Rh proteins, the necessity for such proteins remains a paradox. Based on quantum mechanics and molecular mechanics free energy calculations, we here propose that Rh proteins, like Amt proteins, recruit NH_4^+ at a binding site formed by a signature histidine to which a proton is transferred. We further show that, unlike what is observed in Amts, this excess proton is transferred back to the extracellular side through a network of hydrogen bonds that involves highly conserved aspartic acid (Asp177) and serine (Ser181) residues. Our calculations suggest that, in both Amt and Rh proteins, the histidine dyad acts as a proton acceptor. The two classes of proteins are distinguished by the pathway through which the proton is released, resulting in the net transport of NH_4^+ in Amts and of NH_3 in Rh proteins.

RESULTS

Recruitment of Ammonium and Proton Transfer to His185

By comparison with Amt structures, it was suggested that RhCG lacks a recruitment binding site for ammonium at the extracellular vestibule (Gruswitz et al., 2010; Hub et al., 2010). In Amts, NH_4^+ binds to a site above the phenylalanine gate, at the level of a Trp/Ser pair, but also below the phenylalanine gate, where it interacts with a signature histidine (Wang et al., 2012). The first site, above the phenylalanine gate, has no equivalent in RhCG,

whereas the second one is occupied by a crystallographic water molecule interacting with His185 (Figure 1A). We investigated the binding of ammonium to this site using classical molecular dynamics (MD) simulations. We first performed a 50-ns simulation of the RhCG trimer with one NH_4^+ molecule initially bound to His185 in each pore (restrained to the binding site for the first 5 ns of simulation, then let free to move for the remaining 45 ns). Throughout the trajectory, the ammonium ions remain in the vicinity of His185, with which they interact directly or through a water molecule (Figure 2). The binding affinity of NH_4^+ was calculated as the difference of the free energies for alchemically transforming NH_4^+ into H_2O at this putative recruitment site ($\Delta G = 64.5 \pm 0.5$), and in bulk water ($\Delta G = 59.0 \pm 0.1$). The resulting free energy difference of -5.5 ± 0.5 kcal/mol corresponds to the relative binding free energy of ammonium to the pore. By comparison, the binding affinity at a corresponding site in AmtB was found to be -13 kcal/mol (Wang et al., 2012). The binding affinity difference between the two proteins arises from different coordination schemes. In AmtB, the NH_4^+ coordination shell is tight, with close interactions with aromatic residues and the histidine dyad, and limited interaction with water molecules. In RhCG, NH_4^+ is coordinated by two water molecules, which decreases the relative binding affinity compared with AmtB, as illustrated by the fluctuations of ammonium in its binding site (Figure 2B). Nevertheless, this low-millimolar binding affinity for NH_4^+ in RhCG allows for an efficient recruitment, whereas recruiting NH_3 would be much less efficient because of its lower concentration and lower binding affinity.

Once NH_4^+ is bound to the recruitment site, it is unlikely to diffuse further down since the pore is highly hydrophobic, as was shown by free energy calculation in the homologous Rh50 channel (Hub et al., 2010). Using quantum mechanics (QM)/molecular mechanics (MM) MD simulations, we calculated the potential of mean force (PMF) of the proton transfer from NH_4^+ to His185. The QM region for this calculation is shown in Figure S1A. The resulting free energy profile reveals a reaction free energy of ~2 kcal/mol and a barrier of ~3 kcal/mol (Figure 3). Overall, our calculations suggest that NH_4^+ is recruited at His185 and that a proton can efficiently be exchanged between the bound ammonium and His185.

Dynamics of Substrate after Deprotonation

To investigate the dynamics of ammonia in the pore after deprotonation of ammonium, we simulated RhCG trimer with one ammonia molecule initially placed close to the Nε atom of the
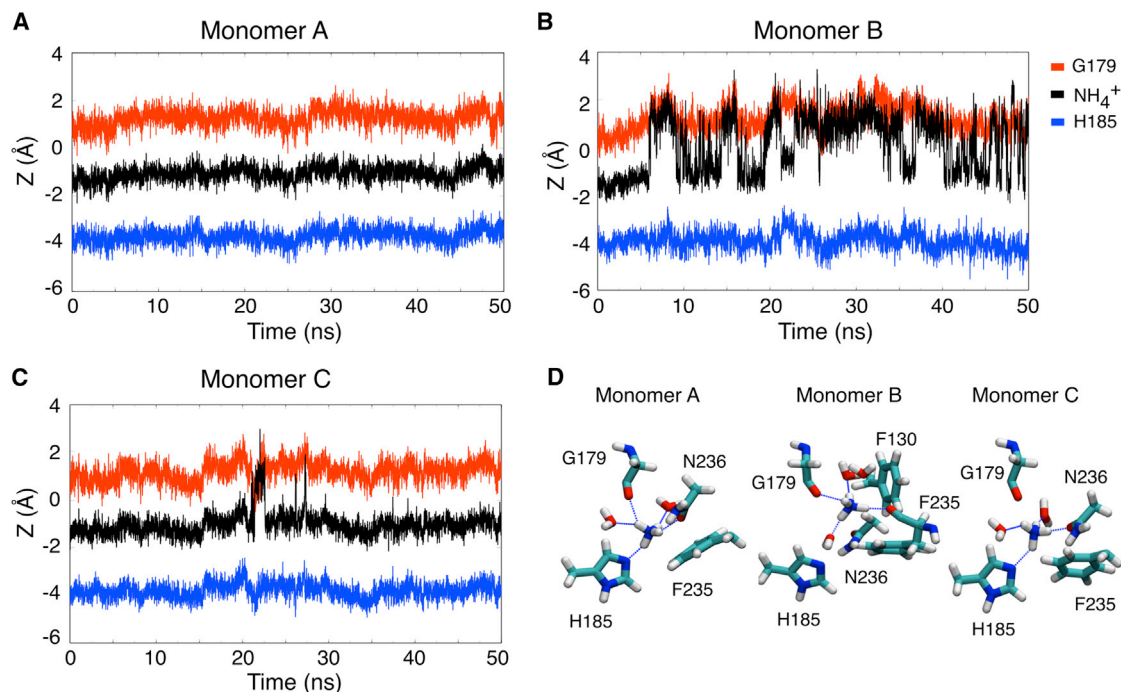
Figure 2. Simulation of RhCG Initiated with an Ammonium Ion Bound to His185 in Each Pore

(A–C) The time series shows the position, along the z axis, of ammonium in the pore of monomer A (A), monomer B (B), and monomer C (C) over the duration of the simulation. For reference, the positions of Gly179 O and His185 Nε atoms are shown. Z = 0 corresponds to the center of mass of Phe130 and Phe235 Cα atoms.

(D) The conformation of the pore of each monomer at the end of the simulation is shown, highlighting key residues and the ammonium ion.

protonated His185. Ammonia was restrained to stay within 3.5 Å of His185 Nε and Gly179 O for the first 5 ns of the 100-ns simulation. As illustrated in Figure 4, once this restraint is removed, ammonia moves to the hydrophobic section of the pore at the level of the two signature histidine residues. In monomers A and C, the ammonia molecule diffuses past Phe74 and His344, while in monomer B it diffuses back to the extracellular bulk. The PMF of ammonia diffusing down the pore was calculated using adaptive biasing force (ABF) simulations (see the Experimental Procedures section). The PMF shown in Figure 4D is in line with the observations based on the unbiased simulations. It further reveals that ammonia is more stable near His185, with free energy barriers of ∼3 kcal/mol opposing the diffusion of NH_3 toward the intra- or extracellular bulk. Overall, the permeation of ammonia across the pore involves relatively low free energy barriers, in agreement with similar PMF obtained for Rh50 (Hub et al., 2010).

Hydrogen Bond Network Linking His185 to Asp177

After deprotonation of NH_4^+, the excess proton on His185 has to be transferred either to the intracellular bulk or back to the extracellular bulk to allow the recruitment of a new ammonium ion. To explore possible proton diffusion pathways, we performed classical simulations of RhCG monomer in which His185 is protonated. We also further analyzed the simulation of the previous section in which His185 is protonated with an ammonia molecule in its vicinity. In these simulations, we observed a dynamic network of hydrogen bonds from His185 to Asp177, involving water molecules and Ser181. In the 50-ns

simulation of RhCG monomer, two similar hydrogen bond networks between His185 and Asp177 are formed in alternation through the simulation. The first of these two networks consists of His185, two water molecules, Ser181 and Asp177, and remains stable up to the 28th ns of the simulation (Figure 5A and 5B). The second network is seen after 32 ns of simulation when the side chain of Ser181 rotates and allows another water molecule to bridge Asp177 with the rest of the network (Figure 5C). In the 100-ns RhCG trimer simulation, the hydrogen bond network forms in two ways. A first one involves direct interaction of Ser181 and Asp177 as illustrated in Figure 5B. This is observed in monomers B and C when the hydrogen bond distance between Ser181 and Asp177 is short (Figure S2A). Monomer A shows another possible network in which a water molecule is connecting Ser181 to Asp177 (Figure S2C). There are thus at least three possible network topologies bridging His185 to Asp177, which differ only in the arrangement of the Ser181 side chain and of the neighboring water molecules. The protonation of His185 appears to favor the formation of stable hydrogen bond networks going from His185 to Asp177, which could potentially facilitate the transport of a proton from the protonated His185 back to the extracellular side.

Proton Transfer from His185 to Asp177

The transfer of a proton through the network of hydrogen bonds connecting the protonated His185 to Asp177 was investigated using QM/MM simulations. Considering the structure presented in Figure 5B, we calculated a two-dimensional PMF from 100 10-ps constrained QM/MM simulations in which the first reaction
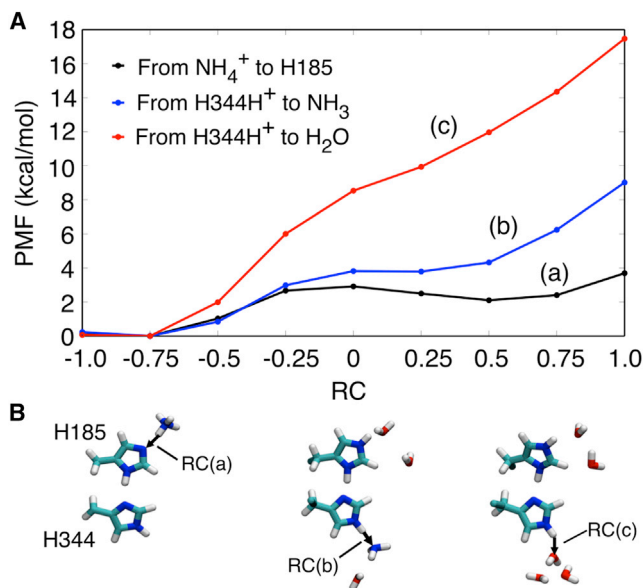
Figure 3. Potentials of Mean Force (PMFs) for Proton Transfer Reactions Occurring in the RhCG Pore Obtained from QM/MM Simulations

(A) The different PMFs correspond to the proton transfer from NH_4^+ to His185 (black (a)), from His344H$^+$ to NH_3 (blue (b)), and from His344H$^+$ to a water molecule (red (c)).

(B) The reaction coordinates (RC(a), RC(b), and RC(c)) of each PMF are defined as RC = $d_{Donor-Proton} - d_{Acceptor-Proton}$. See also Figure S1.

coordinate corresponds to the proton transfer from His185 to a water molecule and the second reaction coordinate to the proton transfer from Ser181 to Asp177. The QM region is illustrated in Figure S1B. The resulting PMF shows that the excess proton on His185 is first transferred to the water molecule, followed by the transfer to Asp177 (Figure 6). The presence of Asp177, which attracts the excess proton, is essential since the transfer of the proton to a water molecule would otherwise be energetically prohibitive (see Figure 3). The free energy barrier corresponds to an H_3O^+ transition state and no local free energy minimum is associated with the presence of such molecule. The free energy difference of the reaction is 9 kcal/mol with a barrier of 16 kcal/mol. This reaction constitutes the rate-limiting step of ammonium transport in RhCG. Assuming an experimental transport rate on the order of 10–100/s, similar to that of AmtB (Zidi-Yahiaoui et al., 2009; Gruswitz et al., 2010; Wacker et al., 2014), the overall activation free energy would be 15.2–16.5 kcal/mol, using Eyring's rate theory with a pre-factor of 1.5×10^{13}/s for proton transfer (see Wang et al., 2012). Thus, the free energy barrier revealed by the QM/MM PMF is consistent with the free energy of activation derived from experimental data.

These calculations suggest that residues Asp177 and Ser181 play a crucial role in the transport of ammonium. The functional study performed by Zidi-Yahiaoui et al. (2009) showed that mutation of Asp177 to asparagine impairs ammonium transport in RhCG protein. Our calculations suggest that mutation of residue Ser181 could have a similar impact. The simulations and free energy calculations we have carried out with His185 in its

protonated state show that Ser181 is likely to be involved in the deprotonation of His185. In the configuration shown in Figure 5C, Ser181 is not directly involved in the proton transfer but it plays a structural role by maintaining Asp177 in position, allowing for the formation of a stable water chain between Asp177 and His185.

When His185 is protonated, it forms with His344 a dyad in which the +1 charge is delocalized. This implies that a proton could potentially be transferred from the His344 Nε atom to a water molecule, or even to the ammonia molecule diffusing down the pore after deprotonation of ammonium, as was discussed for the AmtB transporter (Wang et al., 2012). We used QM/MM simulations to calculate the corresponding PMFs (see Figure 3). While proton transfer to a water molecule seems unlikely, the transfer to NH_3 cannot be excluded with a reaction free energy of 4 kcal/mol (compared with 0.7 kcal/mol for AmtB (Wang et al., 2012)). In that event, a water chain connecting His185 Nε to His344 Nε would be required to re-establish the original protonation state of the two histidines, which is necessary for recruiting a new NH_4^+ (Wang et al., 2012). We carried out a 50-ns simulation of RhCG trimer with protons on His185 Nε and His344 Nδ (neutral histidine dyad) to investigate the possible hydration of the pore. The simulation shows that no chain of water molecules forms in the pore of RhCG under such conditions (Figure S3). Lack of pore hydration when His344 is deprotonated reinforces the idea of a proton release from His185 toward the extracellular side.

Proton Release from Asp177

The free energy of deprotonation of an acid at a given pH can be calculated using the equation:

$$\Delta G^{Deprotonation}(pH) = -2.3kT(pH - pK_a) \quad \text{(Equation 1)}$$

where pK_a is the dissociation constant of the acid, k is the Boltzmann constant, T is the temperature. For an aspartic acid (pK_a of 4.0) in neutral solution, the equation yields a deprotonation free energy of −4.3 kcal/mol (with kT = 0.626 kcal/mol for T = 315 K). To calculate the free energy of releasing a proton from Asp177, we performed free energy perturbation (FEP) calculations that involved the deprotonation of Asp177 and protonation of an aspartic acid dipeptide in bulk solution simultaneously. The starting conformation used for this calculation, obtained after equilibration of the monomeric molecular system with a protonated Asp177, is shown in Figure S4. The FEP calculation provides the free energy difference between the deprotonation of the aspartic acid in the protein and the one in solution $\Delta\Delta G = \Delta G^{Deprotonation}_{Protein} - \Delta G^{Deprotonation}_{Solution} = 0.6 \pm 0.4$ kcal/mol. Taking into account the deprotonation free energy of an aspartic acid in solution, the free energy of releasing a proton from Asp177 to the extracellular solution is −3.7 kcal/mol. This result indicates that the release of a proton from Asp177 to bulk solution is favorable but not as much as the release from an aspartic acid in solution, which is better hydrated.

To close the thermodynamic cycle of transport, we consider that the released proton reacts with NH_3 in solution to form NH_4^+. At pH 7, considering a pK_a of 9.25 for NH_4^+, the reaction free energy is −3.2 kcal/mol. Given the periodic boundary conditions applied to the simulation systems, the overall mechanism should be energetically neutral since both sides of the
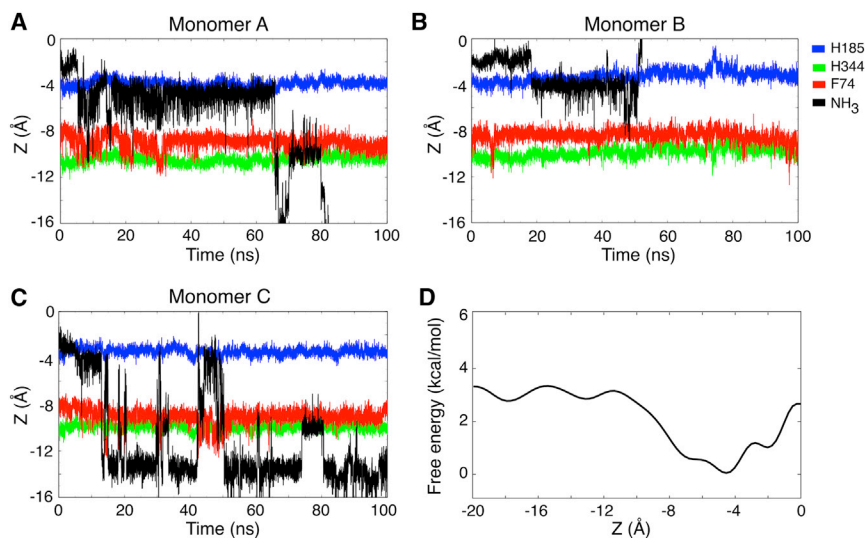
Figure 4. Simulation of RhCG Initiated with One Ammonia Molecule Binding to His185 in Each Pore of the Trimer

The time series shows the position of ammonia along the pore in monomer A (A), monomer B (B), and monomer C (C) during the simulation. The positions of the His185 and His344 Nε atoms and the center of mass of the aromatic ring of Phe74 are shown as reference.

(D) The potential of mean force underlying ammonia diffusion in the hydrophobic pore, obtained by classical MD ABF simulations, reveals a main free energy barrier of ~3 kcal/mol. In all plots, $Z = 0$ corresponds to the center of mass of Phe130 and Phe235 Cα atoms.

membrane are strictly equivalent. In practice, the free energy balance yields a difference of +0.6 kcal/mol, which reflects the precision of the calculation (Table S1).

DISCUSSION

The mechanism by which Rh proteins transport ammonium remains poorly understood. While transport mechanism in Amt proteins is generally thought to involve the recruitment of NH_4^+ followed by its deprotonation, Rh proteins are often assumed, notably based on structural data, to simply facilitate NH_3 diffusion (Hub et al., 2010). Given the low concentration of NH_3 molecules, such a mechanism seems unlikely to have a significant contribution to the overall transport of ammonium (Lupo et al., 2007). Our simulations rather show that RhCG can efficiently recruit NH_4^+ at a site near His185 where electronic density was observed in X-ray crystallography experiments. Using QM/MM simulations, we further showed that a proton can easily transfer from NH_4^+ to His185, with an activation free energy barrier of 3 kcal/mol and a reaction free energy of +2 kcal/mol. The deprotonated substrate, NH_3, can spontaneously reach the hydrophobic pore, through which it diffuses facing free energy barriers of no more than 3 kcal/mol. Simulation studies based on the AmtB structure have proposed mechanisms in which a proton is transferred from NH_4^+ to water molecules and/or an aspartic acid side chain (Lin et al., 2006; Nygaard et al., 2006; Bostick and Brooks, 2007). QM/MM free energy calculations presented here and in previous work (Wang et al., 2012) show that the transfer of a proton from NH_4^+ to any other moieties than the histidine side chain is unlikely because water molecules and side chains such as serine and aspartic acid are poor proton acceptors.

The excess proton transferred from NH_4^+ to His185 prevents the protein from binding an incoming ammonium substrate, and thus, deprotonation of His185 constitutes a key event in the permeation mechanism. As seen for AmtB (Wang et al., 2012), the release of this proton constitutes a kinetic bottleneck. In AmtB, the only accessible proton pathway is through a water chain that transiently forms in the hydrophobic pore, resulting in the net transport of NH_4^+. In RhCG, no such water chain is seen

in the hydrophobic pore, suggesting that net transport of NH_4^+ is unlikely, at odds with reports suggesting that Rh proteins could transport charged ammonium (Bakouh et al., 2004; Nakhoul et al., 2010). However, a hydrogen bond network between His185 and Asp177 allows the proton to diffuse back toward the extracellular side, resulting in net transport of NH_3, in agreement with the bulk of functional data on Rh proteins (Javelle et al., 2007; Weiner and Verlander, 2014). The transfer of a proton from His185 to Asp177, through Ser181, involves a free energy barrier of about 16 kcal/mol, in line with experimental permeation rates (Zidi-Yahiaoui et al., 2009). Asp177 is highly conserved among Amt/Rh proteins and mutation of this residue drastically reduces transport activity in Rh proteins (Marini et al., 2006; Zidi-Yahiaoui et al., 2009) and Amts (Javelle et al., 2004). Given the structural differences between the vestibules of both classes of proteins, the aspartic acid could possibly fulfill different roles. In Amts, it is thought to stabilize the structure around the recruitment site and to be involved in the binding of ammonium (Luzhkov et al., 2006). We propose that in Rh proteins the aspartic acid is involved in proton release from the histidine dyad. Ser181 is highly conserved across the Rh family but only partially conserved in Amts.

Our calculations suggest that, despite their highly similar tridimensional structures, Amt and Rh proteins perform different functions: transport of NH_4^+ for Amts and transport of NH_3 for Rh proteins. In both transport mechanisms, the signature histidine dyad plays a central role as proton acceptor. (Proton transfer from NH_4^+ to any other moiety is thermodynamically unlikely.) The functional difference between the two classes of proteins arises from the proton release, which takes place along a water chain in the hydrophobic pore of Amts, or a hydrogen bond network involving a conserved aspartic acid on the extracellular side of Rh proteins.

EXPERIMENTAL PROCEDURES

Simulation Systems

The RhCG simulation systems were prepared using the crystal structure from PDB: 3HD6 (Gruswitz et al., 2010). RhCG loops that were not resolved (residues 35–52 and 362–383) were modeled using the loop modeling function of the Rosetta program (Wang et al., 2007). Membrane systems of RhCG were built using the CHARMM-GUI Web server (Jo et al., 2008). The molecular systems were prepared by assembling a bilayer composed of 323
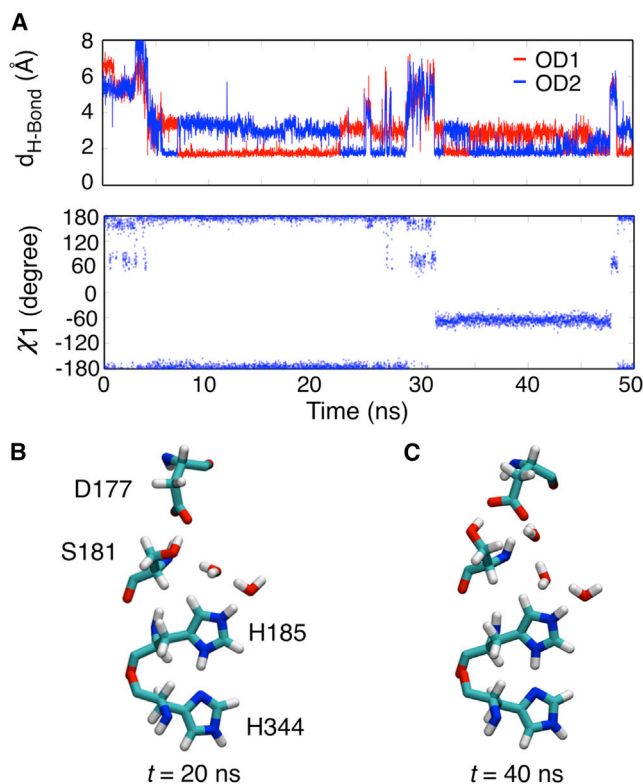
Figure 5. Simulation of RhCG Monomer with H185 Protonated

(A) The upper panel shows the hydrogen bond distance between the Asp177 carboxylate oxygen atoms (OD1 and OD2) and Ser181 hydroxyl group, and the lower panel shows the χ 1 dihedral angle of Ser181.

(B and C) The molecular representations show the hydrogen bond network at $t = 20$ ns (B) and $t = 40$ ns (C). See also Figure S2.

Figure 6. Proton Transfer from His185 to Asp177 through a Network of Hydrogen Bonds Involving Ser181 and Water Molecules

(A) The potential of mean force with the two reaction coordinates defined as RC1 = $d_{His185N\varepsilon-H} - d_{Water-H}$ and RC2 = $d_{Ser181O\gamma-H} - d_{Asp177OD1-H}$ is shown. Each contour level corresponds to 1 kcal/mol.

(B) The molecular representations illustrate the initial a, intermediate b, and final c states, with the reaction coordinates shown in state a. See also Figure S3.

dimyristoylphosphatidylcholine (DMPC) lipid molecules around the RhCG trimer. The systems were solvated with 31,609 TIP3P water molecules, to which 95 K$^+$ and 80 Cl$^-$ ions were added to obtain a salt concentration of about 0.15 M. The tetragonal box of the trimeric systems contained 153,930 atoms, with dimensions of $120 \times 120 \times 104$ Å^3. The trimeric system was used to simulate three different conditions. In the first, an NH$_4^+$ molecule is present in each monomer at the position of the experimental electronic density peak found near His185, with a neutral histidine dyad His185/His344 in which His185 Nε is unprotonated. To equilibrate ammonium at this site, it was restrained to stay within 3.5 Å of the Nε atom of His185 and O atom of Gly179 for the first 5 ns of simulation. In the second system, NH$_4^+$ is replaced by NH$_3$ and a proton is added to His185 Nε. The third system was built on the basis of the second one by removing NH$_3$, transferring a proton from His185 Nδ to His344 Nδ and removing a proton from His344 Nε. To maintain the electroneutrality of this system, three Cl$^-$ ions were also removed. In preparation for the classical and QM/MM free energy simulations, three monomeric systems were prepared, corresponding to the first two trimeric systems, and a third one, in which Asp177 is protonated (see below). An RhCG monomer was assembled with 204 DMPC lipids, 15,813 TIP3P water molecules, and 45 K$^+$ and 40 Cl$^-$ ions. The simulation box with dimensions of $88 \times 88 \times 100$ Å^3 contained 78,538 atoms.

All simulation systems were equilibrated using CHARMM (version 36b1) and production runs were performed using NAMD (version 2.8b3) (Brooks et al., 2009; Phillips et al., 2005). Classical MD simulations were carried out with the CHARMM 27 force field (MacKerell et al., 1998). Electrostatic interactions were calculated using the particle-mesh Ewald method with a grid spacing of ~1 Å (Essmann et al., 1995). Simulations were performed with a time step of 1 fs, with all interactions calculated at every time step. The temperature and pressure normal to the membrane were maintained at 315 K and 1 atm, respectively. The area of the membrane was kept constant.
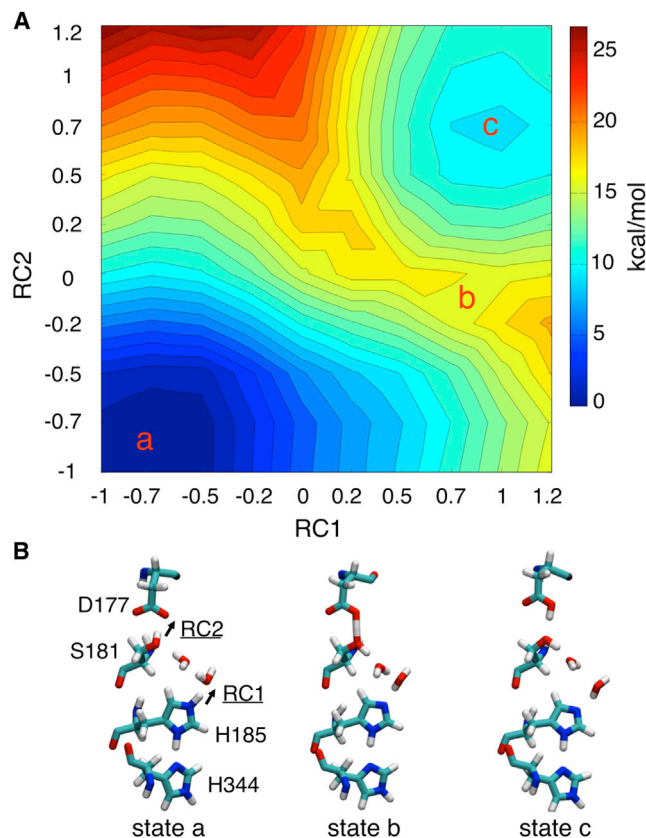
Classical Free Energy Calculations

We performed FEP simulations to evaluate the relative binding free energy of NH$_4^+$ to the pore. The calculation involved the alchemical transformation of NH$_4^+$ into a water molecule at the putative binding site in the protein and in bulk water. The perturbation simulations were performed with a hybrid residue that contains both NH$_4^+$ and a water molecule. Interaction of the hybrid residue with the surrounding environment was controlled using a parameter λ (ranging from 0 to 1). The reaction coordinate for each perturbation simulation was discretized into windows of width 0.1 for λ ranging from 0.1 to 0.9 and these windows were simulated for 400 ps (first 40 ps for equilibration). At the endpoints, λ was progressively increased with windows at 0, 0.001, 0.01, 0.05, and 0.95, 0.99, 0.999, 1 that were simulated for 200 ps (first 20 ps for equilibration). For each perturbation calculation, the combined forward and backward simulations amounted to a total simulation time of 9.6 ns. Free energy differences and statistical errors were calculated by combining the forward and backward configurational ensembles using the Bennett acceptance ratio method as implemented in the ParseFEP toolkit (Liu et al., 2012) of the VMD visualization platform (Humphrey et al., 1996).

We also performed FEP calculations to study the deprotonation of Asp177. The perturbation consisted of the deprotonation of the aspartic acid in the protein combined with the simultaneous protonation of an aspartic acid dipeptide in bulk water. The monomeric system was equilibrated with Asp177 in its protonated state, the histidine dyad in its neutral state with His185 Nε unprotonated, and the addition of a dipeptide in solution away from the protein. This

FEP calculation was carried out using 11 windows, varying λ from 0 to 1 by step of 0.1, $\lambda = 0$ corresponding to the state where the aspartic acid in the protein is protonated and $\lambda = 1$ to the state where the aspartic acid in the solvated dipeptide is protonated. Each window was simulated for 1 ns, with the first 200 ps considered as equilibration. This FEP calculation was performed using the PERT module of CHARMM (Brooks et al., 2009) and the free energy difference was calculated from the combined sampling of forward and backward perturbations using the WHAM module of CHARMM (Souaille and Roux, 2001).

PMFs for NH_3 diffusing through the hydrophobic pore were calculated using the ABF method of the NAMD program (Darve and Pohorille, 2001; Hénin and Chipot, 2004). The reaction coordinate was defined as the distance along the z axis between the nitrogen of NH_3 and the center of mass of the $C\alpha$ atoms of Phe130 and Phe235. The reaction coordinate covering 20 Å was divided into four equidistant windows. Each window was simulated for 25 ns. Colvars module of NAMD was used to restrain NH_3 along the reaction coordinate. Biasing forces were applied and accumulated after 5,000 steps of simulation.

Quantum Mechanics/Molecular Mechanics Simulations

PMFs of proton transfer reactions were obtained from constrained QM/MM simulations. The QM/MM simulations were performed using the CP2K program (Laino et al., 2005) following the protocol described in Wang et al. (2012). The reaction coordinate (RC) for a proton transfer is defined as the difference of the distances from the proton to the acceptor and donor atoms:

$$RC = d_{Acceptor-H} - d_{Donor-H}$$

1D PMFs were calculated using ten windows with RC = (-1, -0.75, -0.5, -0.25, 0, 0.25, 0.5, 0.75, 1.0, 1.25) and a simulation time of 10 ps per window. The 2D PMF was obtained from simulations of 100 windows (combination of two reaction coordinations having ten windows each) and each window was simulated for 10 ps. The proton was constrained according to the RC value and constraint forces acting on the proton were collected. The 2D PMF is obtained from the average forces using the single-sweep reconstruction method of Maragliano and Vanden-Eijnden (2008). The optimal PMF corresponds to a weighted sum of radial Gaussian distributions with $\sigma = 0.315$ Å. Force data for the first 2 ps of the simulations were considered as equilibration and were not used in the calculation of the PMFs.

In the PMF simulations for the proton transfer from NH_4^+ to His185, the QM region includes the peptide bond between Gly179 and Gly180, the side chains of His185, His344, Trp232, Phe235, and Asn236, as well as a water molecule interacting with NH_4^+. In the PMF simulations for the proton transfer from H344 to either ammonia or water, the QM region contains the proton acceptor (ammonia or water molecule), the side-chain atoms of H185 and H344, and water molecules around these atoms. The QM region of the 2D PMF simulations contains the atoms of side chains of His185, His344, Asn236, the complete residues from position 177 to 181, the peptide bond between Val291 and Ala292, and two key water molecules. Initial structures of the QM regions for the PMF simulations are given in Figure S1.

SUPPLEMENTAL INFORMATION

Supplemental Information includes four figures and one table and can be found with this article online at http://dx.doi.org/10.1016/j.str.2015.06.010.

AUTHOR CONTRIBUTIONS

S. Bernèche and G.L. conceived and designed the computational experiments and calculations; S. Baday and E.A.O. performed the simulations; S. Baday, E.A.O., and S.W. analyzed the data; S. Baday, S. Bernèche, and G.L. co-wrote the article.

REFERENCES

Andrade, S.L., Dickmanns, A., Ficner, R., and Einsle, O. (2005). Crystal structure of the archaeal ammonium transporter Amt-1 from *Archaeoglobus fulgidus*. Proc. Natl. Acad. Sci. USA *102*, 14994–14999.

Baday, S., Wang, S., Lamoureux, G., and Bernèche, S. (2013). Different hydration patterns in the pores of AmtB and RhCG could determine their transport mechanisms. Biochemistry *52*, 7091–7098.

Bakouh, N., Benjelloun, F., Hulin, P., Brouillard, F., Edelman, A., Chérif-Zahar, B., and Planelles, G. (2004). NH3 is involved in the NH4+ transport induced by the functional expression of the human Rh C glycoprotein. J. Biol. Chem. *279*, 15975–15983.

Benjelloun, F., Bakouh, N., Fritsch, J., Hulin, P., Lipecka, J., Edelman, A., Planelles, G., Thomas, S.R., and Chérif-Zahar, B. (2005). Expression of the human erythroid Rh glycoprotein (RhAG) enhances both NH3 and NH4+ transport in HeLa cells. Pflugers Arch. *450*, 155–167.

Bostick, D.L., and Brooks, C.L. (2007). On the equivalence point for ammonium (de)protonation during its transport through the AmtB channel. Biophys. J. *92*, L103–L105.

Brooks, B.R., Brooks, C.L., Mackerell, A.D., Nilsson, L., Petrella, R.J., Roux, B., Won, Y., Archontis, G., Bartels, C., Boresch, S., et al. (2009). CHARMM: the biomolecular simulation program. J. Comput. Chem. *30*, 1545–1614.

Darve, E., and Pohorille, A. (2001). Calculating free energies using average force. J. Chem. Phys. *115*, 9169–9183.

Essmann, U., Perera, L., Berkowitz, M.L., Darden, T., Lee, H., and Pedersen, L.G. (1995). A smooth particle mesh Ewald method. J. Chem. Phys. *103*, 8577–8593.

Gruswitz, F., Chaudhary, S., Ho, J.D., Schlessinger, A., Pezeshki, B., Ho, C.-M.M., Sali, A., Westhoff, C.M., and Stroud, R.M. (2010). Function of human Rh based on structure of RhCG at 2.1 A. Proc. Natl. Acad. Sci. USA *107*, 9638–9643.

Hemker, M.B., Cheroutre, G., van Zwieten, R., Maaskant-van Wijk, P.A., Roos, D., Loos, J.A., van der Schoot, C.E., and von dem Borne, A.E. (2003). The Rh complex exports ammonium from human red blood cells. Br. J. Haematol. *122*, 333–340.

Hénin, J., and Chipot, C. (2004). Overcoming free energy barriers using unconstrained molecular dynamics simulations. J. Chem. Phys. *121*, 2904–2914.

Hub, J.S., Winkler, F.K., Merrick, M., and de Groot, B.L. (2010). Potentials of mean force and permeabilities for carbon dioxide, ammonia, and water flux across a rhesus protein channel and lipid membranes. J. Am. Chem. Soc. *132*, 13251–13263.

Humphrey, W., Dalke, A., and Schulten, K. (1996). VMD: visual molecular dynamics. J. Mol. Graph. *14*, 33–38.

Javelle, A., Severi, E., Thornton, J., and Merrick, M. (2004). Ammonium sensing in *Escherichia coli*. Role of the ammonium transporter AmtB and AmtB-GlnK complex formation. J. Biol. Chem. *279*, 8530–8538.

Javelle, A., Thomas, G., Marini, A.M., Krämer, R., and Merrick, M. (2005). In vivo functional characterization of the *Escherichia coli* ammonium channel AmtB: evidence for metabolic coupling of AmtB to glutamine synthetase. Biochem. J. *390*, 215–222.

Javelle, A., Lupo, D., Li, X.-D.D., Merrick, M., Chami, M., Ripoche, P., and Winkler, F.K. (2007). Structural and mechanistic aspects of Amt/Rh proteins. J. Struct. Biol. *158*, 472–481.

Jo, S., Kim, T., Iyer, V.G., and Im, W. (2008). CHARMM-GUI: a web-based graphical user interface for CHARMM. J. Comput. Chem. *29*, 1859–1865.

Khademi, S., O'Connell, J., Remis, J., Robles-Colmenares, Y., Miercke, L.J., and Stroud, R.M. (2004). Mechanism of ammonia transport by Amt/MEP/Rh: structure of AmtB at 1.35 A. Science *305*, 1587–1594.

Laino, T., Mohamed, F., Laio, A., and Parrinello, M. (2005). An efficient real space multigrid QM/MM electrostatic coupling. J. Chem. Theor. Comput. *1*, 1176–1184.

Lin, Y., Cao, Z., and Mo, Y. (2006). Molecular dynamics simulations on the *Escherichia coli* ammonia channel protein AmtB: mechanism of ammonia/ammonium transport. J. Am. Chem. Soc. *128*, 10876–10884.

Liu, P., Dehez, F.O., Cai, W., and Chipot, C. (2012). A toolkit for the analysis of free-energy perturbation calculations. J. Chem. Theor. Comput. *8*, 2606–2616.

Ludewig, U. (2004). Electroneutral ammonium transport by basolateral rhesus B glycoprotein. J. Physiol. *559*, 751–759.

Ludewig, U., von Wirén, N., and Frommer, W.B. (2002). Uniport of NH4+ by the root hair plasma membrane ammonium transporter LeAMT1;1. J. Biol. Chem. *277*, 13548–13555.

Lupo, D., Li, X.-D.D., Durand, A., Tomizaki, T., Cherif-Zahar, B., Matassi, G., Merrick, M., and Winkler, F.K. (2007). The 1.3-A resolution structure of *Nitrosomonas europaea* Rh50 and mechanistic implications for NH3 transport by rhesus family proteins. Proc. Natl. Acad. Sci. USA *104*, 19303–19308.

Luzhkov, V.B., Almlöf, M., Nervall, M., and Aqvist, J. (2006). Computational study of the binding affinity and selectivity of the bacterial ammonium transporter AmtB. Biochemistry *45*, 10807–10814.

MacKerell, A.D., Jr., Bashford, D., Bellott, M., Dunbrack, R.L., Jr., Evanseck, J.D., Field, M.J., Fischer, S., Gao, J., Guo, H., and Ha, S. (1998). All-atom empirical potential for molecular modeling and dynamics studies of proteins. J. Phys. Chem. B *102*, 3586–3616.

Maragliano, L., and Vanden-Eijnden, E. (2008). Single-sweep methods for free energy calculations. J. Chem. Phys. *128*, 184110.

Marini, A.M., Soussi-Boudekou, S., Vissers, S., and Andre, B. (1997). A family of ammonium transporters in *Saccharomyces cerevisiae*. Mol. Cell. Biol. *17*, 4282–4293.

Marini, A.M., Boeckstaens, M., Benjelloun, F., Chérif-Zahar, B., and André, B. (2006). Structural involvement in substrate recognition of an essential aspartate residue conserved in Mep/Amt and Rh-type ammonium transporters. Curr. Genet. *49*, 364–374.

Mouro-Chanteloup, I., Cochet, S., Chami, M., Genetet, S., Zidi-Yahiaoui, N., Engel, A., Colin, Y., Bertrand, O., and Ripoche, P. (2010). Functional reconstitution into liposomes of purified human RhCG ammonia channel. PLoS One *5*, e8921.

Nakhoul, N.L., Dejong, H., Abdulnour-Nakhoul, S.M., Boulpaep, E.L., Hering-Smith, K., and Hamm, L.L. (2005). Characteristics of renal Rhbg as an NH4(+) transporter. Am. J. Physiol. Renal Physiol. *288*, F170–F181.

Nakhoul, N.L., Abdulnour-Nakhoul, S.M., Boulpaep, E.L., Rabon, E., Schmidt, E., and Hamm, L.L. (2010). Substrate specificity of Rhbg: ammonium and methyl ammonium transport. Am. J. Physiol. Cell Physiol. *299*, C695–C705.

Ninnemann, O., Jauniaux, J.C., and Frommer, W.B. (1994). Identification of a high affinity NH4+ transporter from plants. EMBO J. *13*, 3464–3471.

Nygaard, T.P., Rovira, C., Peters, G.H., and Jensen, M. (2006). Ammonium recruitment and ammonia transport by *E. coli* ammonia channel AmtB. Biophys. J. *91*, 4401–4412.

Phillips, J.C., Braun, R., Wang, W., Gumbart, J., Tajkhorshid, E., Villa, E., Chipot, C., Skeel, R.D., Kalé, L., and Schulten, K. (2005). Scalable molecular dynamics with NAMD. J. Comput. Chem. *26*, 1781–1802.

Ripoche, P., Bertrand, O., Gane, P., Birkenmeier, C., Colin, Y., and Cartron, J.-P.P. (2004). Human rhesus-associated glycoprotein mediates facilitated transport of NH(3) into red blood cells. Proc. Natl. Acad. Sci. USA *101*, 17222–17227.

Siewe, R.M., Weil, B., Burkovski, A., Eikmanns, B.J., Eikmanns, M., and Krämer, R. (1996). Functional and genetic characterization of the (methyl)ammonium uptake carrier of *Corynebacterium glutamicum*. J. Biol. Chem. *271*, 5398–5403.

Souaille, M., and Roux, B.T. (2001). Extension to the weighted histogram analysis method: combining umbrella sampling with free energy calculations. Comput. Phys. Commun. *135*, 40–57.

Ullmann, R.T., Andrade, S.L., and Ullmann, G.M. (2012). Thermodynamics of transport through the ammonium transporter Amt-1 investigated with free energy calculations. J. Phys. Chem. B *116*, 9690–9703.

Wacker, T., Garcia-Celma, J.J., Lewe, P., and Andrade, S.L. (2014). Direct observation of electrogenic NH4(+) transport in ammonium transport (Amt) proteins. Proc. Natl. Acad. Sci. USA *111*, 9995–10000.

Wang, C., Bradley, P., and Baker, D. (2007). Protein–protein docking with backbone flexibility. J. Mol. Biol. *373*, 503–519.

Wang, S., Orabi, E.A., Baday, S., Bernèche, S., and Lamoureux, G. (2012). Ammonium transporters achieve charge transfer by fragmenting their substrate. J. Am. Chem. Soc. *134*, 10419–10427.

Weiner, I.D., and Verlander, J.W. (2014). Ammonia transport in the kidney by rhesus glycoproteins. Am. J. Physiol. Renal Physiol. *306*, F1107–F1120.

Zheng, L., Kostrewa, D., Bernèche, S., Winkler, F.K., and Li, X.D. (2004). The mechanism of ammonia transport based on the crystal structure of AmtB of *Escherichia coli*. Proc. Natl. Acad. Sci. USA *101*, 17090–17095.

Zidi-Yahiaoui, N., Callebaut, I., Genetet, S., Le Van Kim, C., Cartron, J.P., Colin, Y., Ripoche, P., and Mouro-Chanteloup, I. (2009). Functional analysis of human RhCG: comparison with *E. coli* ammonium transporter reveals similarities in the pore and differences in the vestibule. Am. J. Physiol. Cell Physiol. *297*, C537–C547.